Istraživanja i projektovanja za privredu
ISSN 1451-4117
DOI:10.5937/jaes0-37006
www.engineeringscience.rs

iipp publishing

Journal of Applied Engineering Science
Vol. 20, No. 4, 2022
Original Scientific Paper
Paper number: 20(2022)4, 1023,1184-1195

THERMAL PERFORMANCE OF WAX TROMBE WALL

Hussein M. Salih*, Adel H. Ayaal

Electromechanical Engineering Department, University of Technology, Baghdad, Iraq
** 50004@uotechnology.edu.iq*

Using solar energy to cover heating loads of building is a clean and unconventional way that can help reduce electricity consumption. Problems of the cost of energy and environmental pollution are among the most important challenges facing humanity at the present time. And as most of the energy is used for heating and ventilation, thus the need to find renewable sources of energy has become a pressing need. In this direction Trombe wall, which is a classical passive solar wall, has become one of the most important heating and ventilation technologies of buildings. In the present work a three-dimensional numerical study of thermal energy performance for Trombe wall utilizing paraffin wax as PCM was presented. The effect of PCM thickness was studied as (2, 3, 4 and 5 cm). A FORTRAN-90 computer program was built to solve a three-dimensional, turbulent Navier stokes and energy equations in addition to enthalpy transforming method for PCM with explicit scheme based on finite volume method. Numerical results of the present code were validated by comparing them with previous experimental results and a good agreement was noted. The results show that a 2 cm thick PCM is an optimal thickness, where the percentage rates of increasing in air temperature over ambient temperature at day hours (10 am, 12 pm, 5 pm, 10 pm and 7 am of the next day) were (37.8, 19.5, 30.7, 60 and 69.2%) respectively, compared to (33.5, 15.2, 25.9, 53.3 and 65.3) % respectively for a 5 cm wax calculated at the same hours.

Keywords: trombe wall, phase change materials (PCMs), CFD, thermal storage wall, latent heat storage

1 INTRODUCTION

The construction of modern buildings is linked to two main factors, namely sustainable development and the provision of the necessary energy [1, 2]. The use of solar energy to cover building heating loads is unconventional clean way that can help reduce electricity consumption. Therefore, buildings must be designed to suit the climate of that [3, 4]. Trombe wall is considered as one of the passive solar heating methods, which can help provide heating for the space all day, especially at night. Comparing heating methods of rooms by direct gain and the use of Trombe wall technology, uniformity in temperature in spaces utilizing Trombe wall was noticed [5]. So Trombe wall has been studied in a lot of researches, which noted that thermal performance was a function of different parameters such as area and thickness of the wall, orientation, glass thickness, and area of the sun space. In the following paragraphs, some of these studies will be reviewed.

Limited thermal storage capacity, reduces the efficiency of Trombe wall to work at night, and in order to avoid this, Liu et al. [6] studied the use of PCM to improve thermal performance of Trombe wall during night hours. MATLAB was used to simulate an unsteady heat transfer utilizing PCM in Trombe wall. The effect of the external design of the insulation on the thermal performance was studied. From the experimental results, thermal comfort factors within the space were neutralized by using passive solar energy. Elghamry and Hassan [7] presented an experimental study for heating in building by using Trambe wall combined with renewable energy system. Solar chimney with PV inside it and geothermal energy was utilized in order to heat outside air before entering the room. From this study it was noted that the maximum power obtained from PV inside the chimney was 75.1% of the PV power outside. Wu et al. [8] studied heating and ventilating performance of PV- Trombe wall with air purgation. The effect of channel dimensions on the thermal and electrical performance and the performance of the PC-PV-Trombe was studied. The study was conducted for a number of ambient temperatures and solar radiation intensity. The results showed that clean air flow rate, thermal and electrical efficiencies and heat output for the PC-PV-Trombe wall have various trends of reduction or growing with the change of channel dimension. Salih et al. [9] presented a numerical study of a novel solar air heater consisting of two numerical models to simulate thermal behavior for a collector with and without PCM. A finite volume method was employed in mathematical analysis of the governing equation and enthalpy transforming method for PCM utilizing explicit scheme. The effects of air flow and heat flux were studied. Hu et al. [10] studied the effectiveness of water blind Trombe wall system in heating and ventilation theoretically and experimentally. The results showed that in winter, Water-Trombe wall system showed adequate insulation with the average heat transfer coefficient of 0.8 W/m2 K, while Trombe wall lowered the temperature about 13.6% compared with cooling water system with annual energy collection of 20.3 kWh. A new shape for the channel inlet and outlet that features the quadratic Bezier curve was suggested by Wu et al. [11] to enhance solar dual catalytic Trombe wall performance. The study adopted a two-dimensional numerical model. The effect of duct dimensions of height and depth on the thermal performance in addition to air purification performance of solar dual catalytic Trombe wall was studied for several values of solar irradiation intensities. From results, solar dual catalytic Trombe wall with traditional shapes of inlet and outlet showed a decrease in thermal efficiency with increasing channel width while there was no noticeable effect with the channel height. Omara and Abuelnuor [12] presented an extensive review on the various advantages of using PCMs Trombe walls. The article showed that heat storage capacity was adequate because PCM can

effectively increase the thermal circulation of indoor air and reduce fluctuations in indoor air temperature. Moreover, the effectiveness of PCM in providing overheating protection, improving energy efficiency management and energy-saving process of Trombe walls was noticed. Energy Efficiency and Thermal Performance of Trombe Wall of lightweight steel frame was evaluated by Lohmann and Santos [13]. The measurements were made inside two identical real cubic units, exposed for normal outdoor weather conditions. The results were simulated numerically. A steady state thermal performance of a composite Trombe wall was investigated by Zhou et al.[14]. Three types of Trombe walls were examined: traditional, water, and glass-water. The Water type showed the best efficiency during daytime and also during night-time. Hu et al.[15] proposed an experimental and numerical study of a novel water blind-Trombe wall system. In addition to the uses of this new type of Trombe wall for heating and ventilation, it is also used to heat water. By comparison with traditional, the ability of the new design was observed to provide adequate insulation during the winter season, in addition to making use of unwanted solar radiation during the summer to heat water for domestic use. Thermal performance of a Trombe wall with an integrated Venetian blind during the winter was predicted by Hong et al. [16]. From results, venetian blind integrated TW was more efficient to overcome overheating through ventilation and shading, in additional to the more efficient ventilation. The effect of using porous media and fan on the thermal performance of hybrid photovoltaic and Trombe wall were investigated theoretically and experimentally by Ahmed et al. [17]. They concluded that the using of porous material and fan has a significant effect on the system performance while it has an unfavorable effect on the glass cover. Moreover, using the porous medium with fan developed the thermal and electrical efficiencies about 13% and 4%, respectively. A classic Trombe wall was studied by Ana Briga et al. [18] under realistic climatic conditions in a Portuguese city. Shading devices and ventilation openings and their effect on temperature fluctuations were studied. In case of closing the ventilation system and inactivated shading device, the indoor temperatures exceeded the outside temperature value in 9°C. This indicates the system's ability to store and release heat.

In the present study, a numerical analysis for a Trombe wall utilizing Paraffin wax as PCM will be investigated. A three dimensional Navier Stokes equations and enthalpy transforming method for PCM with explicit scheme based on finite volume method will be considered. Thickness of PCM wall will be studied to predict an optimal thickness, which ensure suitable rise in air temperature with a stability of temperature all day, especially at night.

2 PHYSICAL MODEL

The studied physical model consists of the following items: a glass plate 4 mm thick; an air gap thickness of 4 cm; a wall consists of: an absorber plate 5 mm thick; thickness of paraffin wax was changed (2, 3, 4 and 5 cm), wall dimension: 1 m width and 2.5 m height. Fig. 1 shows the physical model scheme. As for the wax used, Table 1 illustrates the thermo-physical properties for Iraqi paraffin wax which considered in the present study [19].

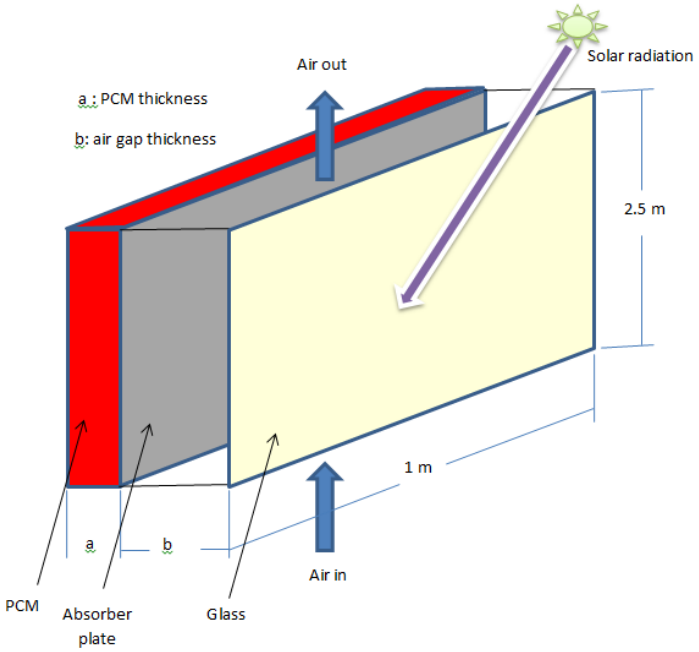

Fig. 1. Physical model scheme

Table 1. Thermo-physical properties for Iraqi paraffin wax

Material Property	Range
Melting temperature [^{o}C]	40
Latent heat of fusion [kJ/kg]	190
Solid-liquid density [kg/m^{3}]	930/830

Material Property	Range
Thermal conductivity [W/m °C]	0.21
Solid, specific heat (*cws*) [kJ/kg °C]	2.384
Liquid, specific heat (*cwl*) [kJ/kg °C]	2.49

1 MATHEMATICAL FORMULATION

In the present study, there are two domains for solution. One of them is the air passage between glass and wall, while the other one is the wall with paraffin wax. The governing equation will be summarized as follow:

1.1 Airway between glass and wall

A three-dimensional Navier stokes equation with energy equation in addition to the k-ε turbulence model will be solved by finite volume method. The governing equations are as follow [20]:

1-Continuity Equation:

$$\frac{\partial u}{\partial x}+\frac{\partial v}{\partial y}+\frac{\partial w}{\partial z}=0 \tag{1}$$

2-Momentum Equation:

x-direction

$$\frac{\partial}{\partial x}(uu)+\frac{\partial}{\partial y}(uv)+\frac{\partial y}{\partial z}(uw)=-\frac{1}{\rho}\frac{\partial P}{\partial x}+v_e\left(\frac{\partial^2 u}{\partial x^2}+\frac{\partial^2 u}{\partial y^2}+\frac{\partial^2 u}{\partial z^2}\right) \tag{2}$$

y-direction

$$\frac{\partial}{\partial x}(vu)+\frac{\partial}{\partial y}(vv)+\frac{\partial}{\partial z}(vw)=-\frac{1}{\rho}\frac{\partial P}{\partial y}+v_e\left(\frac{\partial^2 v}{\partial x^2}+\frac{\partial^2 v}{\partial y^2}+\frac{\partial^2 v}{\partial z^2}\right)+\beta g(T-T_W) \tag{3}$$

z-direction

$$\frac{\partial}{\partial x}(uw)+\frac{\partial}{\partial y}(vw)+\frac{\partial}{\partial z}(ww)=-\frac{1}{\rho}\frac{\partial P}{\partial z}+v_e\left(\frac{\partial^2 w}{\partial x^2}+\frac{\partial^2 w}{\partial y^2}+\frac{\partial^2 w}{\partial z^2}\right) \tag{4}$$

3-Energy Equation

$$\frac{\partial}{\partial x}(uT)+\frac{\partial}{\partial y}(vT)+\frac{\partial}{\partial z}(wT)=\frac{k}{\rho C_p}\left(\frac{\partial^2 T}{\partial x^2}+\frac{\partial^2 T}{\partial y^2}+\frac{\partial^2 T}{\partial z^2}\right) \tag{5}$$

4- k-ε turbulence model

k-ε turbulence model, can be written in a general form as [20].

$$\frac{\partial}{\partial x}(\rho u\varphi)+\frac{\partial}{\partial y}(\rho v\varphi)+\frac{\partial y}{\partial z}(\rho w\varphi)=\frac{\partial}{\partial x}\left(\Gamma_\varphi\frac{\partial \varphi}{\partial x}\right)+\frac{\partial}{\partial y}\left(\Gamma_\varphi\frac{\partial \varphi}{\partial y}\right)+\frac{\partial}{\partial z}\left(\Gamma_\varphi\frac{\partial \varphi}{\partial z}\right)+S_\varphi \tag{6}$$

Where φ:: refers to k or ε

$\Gamma_k=\frac{v_t}{\sigma_k}$; $\Gamma_\varepsilon=\frac{v_t}{\sigma_\varepsilon}$; $S_k=G-\varepsilon$; $S_\varepsilon=C_{1\varepsilon}\frac{\varepsilon}{k}G-C_{2\varepsilon}\frac{\varepsilon^2}{k}$ and the empirical constants for standard k-ε turbulence model are: $C_\mu=0.09$, $C_{1\varepsilon}=1.44$, $C_{2\varepsilon}=1.92$, $\sigma_k=1.00$, $\sigma_\varepsilon=1.30$.

1.2 Wall with Paraffin Wax

Heat conduction with phase change will be presented by Stefan problems. This method is based on enthalpy transforming method. By this method, energy equation is converted into nonlinear equation, where the enthalpy is the single dependent variable. This method is characterized by its ability to solve the problem when formulated in a fixed area. In addition to this, enthalpy is treated as a dependent variable in addition to temperature. The energy equation is separated into a system of equations including both temperature and enthalpy.

Some assumptions will be made in this method, as follow:

- Three dimensional transient heat transfer
- Viscous dissipation will be neglected
- Radiation and convection terms will be neglected
- Specific heats assumed to be constant for each phase, where the phase change takes place at a single temperature

Thus, the energy equation will be [21].

$$\frac{\partial}{\partial x}\left(k\frac{\partial T}{\partial x}\right)+\frac{\partial}{\partial y}\left(k\frac{\partial T}{\partial y}\right)+\frac{\partial}{\partial z}\left(k\frac{\partial T}{\partial z}\right)+\overline{q}\ =\rho\frac{\partial \mathrm{H}}{\partial \mathrm{t}} \tag{7}$$

The state equation

$$\frac{\mathrm{dH}}{\mathrm{dT}}=\mathrm{C_p(T)} \tag{8}$$

For each phase, specific heat is constant and the change of phase take place at a single temperature [22, 23].

$$T=\begin{cases} T_m+{}^{H}/_{C_s} & H\le 0 \quad (Soild\ phase)\\ T_m & 0<H<L \quad (Phase\ change)\\ T_m+{}^{(H-L)}/_{C_l} & H\ge L \quad (Liquid\ phase)\end{cases} \tag{9}$$

Where at H=0 this referred to solid phase of PCM,

For the above relation, H = 0 was selected according to the phase change material (PCM) in their solid state to temperature Tm.

Also, the "Kirchhoff" temperature is presented as [24].

$$T^*=\int_{T_m}^{T}k(\eta)d\eta=\begin{cases}k_s(T-T_m), & T<T_m\\ 0, & T=T_m\\ k_l(T-T_m), & T>T_m\end{cases} \tag{10}$$

Utilizing equation (9) with the definition illustrated in equation (10).

$$\mathrm{T^*}=\begin{cases}{}^{\mathrm{k_sH}}/_{\mathrm{C_s}}, & \mathrm{H}\le 0\\ 0, & 0<\mathrm{H}<\mathrm{L}\\ {}^{\mathrm{k_l(H-L)}}/_{\mathrm{C_l}}, & \mathrm{H}\ge \mathrm{L}\end{cases} \tag{11}$$

Thus, enthalpy function can be introducing as:

$$\mathrm{T^*=\lambda(H)H+S(H)} \tag{12}$$

And changing in phase at a particular temperature,

$$\lambda(\mathrm{H})=\begin{cases}\frac{\mathrm{k_s}}{\mathrm{C_{ps}}}, & \mathrm{H}\le 0\\ 0, & 0<\mathrm{H}<\mathrm{L}\\ \frac{\mathrm{k_l}}{\mathrm{C_{pl}}}, & \mathrm{H}\ge \mathrm{L}\end{cases} \tag{13}$$

With

$$\mathrm{S(H)}=\begin{cases}0, & \mathrm{H}\le 0\\ 0, & 0<\mathrm{H}<\mathrm{L}\\ -\frac{\mathrm{Lk_l}}{\mathrm{C_{pl}}}, & \mathrm{H}\ge \mathrm{L}\end{cases} \tag{14}$$

Substituting equation (12) in equation (7) yield:

$$\rho\frac{\partial \mathrm{H}}{\partial \mathrm{t}}=\frac{\partial}{\partial \mathrm{x}}\left(\frac{\partial(\lambda \mathrm{H})}{\partial \mathrm{x}}\right)+\frac{\partial}{\partial \mathrm{y}}\left(\frac{\partial(\lambda \mathrm{H})}{\partial \mathrm{y}}\right)+\frac{\partial}{\partial \mathrm{z}}\left(\frac{\partial(\lambda \mathrm{H})}{\partial \mathrm{z}}\right)+\mathrm{p}+\mathrm{q} \tag{15}$$

With:

$$\mathrm{p}=\frac{\partial}{\partial \mathrm{x}}\left(\frac{\partial S}{\partial \mathrm{x}}\right)+\frac{\partial}{\partial \mathrm{y}}\left(\frac{\partial S}{\partial \mathrm{y}}\right)+\frac{\partial}{\partial \mathrm{z}}\left(\frac{\partial S}{\partial \mathrm{z}}\right) \tag{16}$$

For liquid region, equation (15) can be reduced to the following formula:

$$\rho\frac{\partial \mathrm{H}}{\partial \mathrm{t}}=\frac{\partial}{\partial \mathrm{x}}\left(\mathrm{k_l}\frac{\partial \mathrm{T}}{\partial \mathrm{x}}\right)+\frac{\partial}{\partial \mathrm{y}}\left(\mathrm{k_l}\frac{\partial \mathrm{T}}{\partial \mathrm{y}}\right)+\frac{\partial}{\partial \mathrm{z}}\left(\mathrm{k_l}\frac{\partial \mathrm{T}}{\partial \mathrm{z}}\right)+\mathrm{q} \tag{17}$$

While for solid region, equation (15) becomes:

$$\rho\frac{\partial \mathrm{H}}{\partial \mathrm{t}}=\frac{\partial}{\partial \mathrm{x}}\left(\mathrm{k_s}\frac{\partial \mathrm{T}}{\partial \mathrm{x}}\right)+\frac{\partial}{\partial \mathrm{y}}\left(\mathrm{k_s}\frac{\partial \mathrm{T}}{\partial \mathrm{y}}\right)+\frac{\partial}{\partial \mathrm{z}}\left(\mathrm{k_s}\frac{\partial \mathrm{T}}{\partial \mathrm{z}}\right)+\mathrm{q} \tag{18}$$

Within the PCM without convection, equation (15) is reduced to:

$$\rho\frac{\partial H}{\partial t}=\frac{\partial^2}{\partial x^2}(\lambda H)+\frac{\partial S^2}{\partial x^2}+\frac{\partial^2}{\partial y^2}(\lambda H)+\frac{\partial^2 S}{\partial y^2}+\frac{\partial^2}{\partial z^2}(\lambda H)+\frac{\partial^2 S}{\partial y^2}+q \quad (19)$$

And for $\lambda=\lambda(H)$ and S=S (H), the above equations can be evaluated by finite volume method with utilizing explicit scheme, thus equation (19) can be written in the discretization form as [25].

$$a_pH_p=a_EH_E+a_WH_W+a_TH_T+a_BH_B+a_SH_S+a_NH_N+b \quad (20)$$

Where:

$$a_E=\frac{\Delta t}{\rho\Delta V}\frac{\lambda_E A_x}{\delta x_e},a_W=\frac{\Delta t}{\rho\Delta V}\frac{\lambda_W A_x}{\delta x_w},a_T=\frac{\Delta t}{\rho\Delta V}\frac{\lambda_T A_y}{\delta y_T},a_B=\frac{\Delta t}{\rho\Delta V}\frac{\lambda_B A_y}{\delta y_B},a_S=\frac{\Delta t}{\rho\Delta V}\frac{\lambda_S A_z}{\delta z_S},\ a_N=\frac{\Delta t}{\rho\Delta V}\frac{\lambda_N A_z}{\delta z_N}$$

$$a_p=a_E+a_W+a_T+a_B+a_S+a_N$$

$$A_x=\Delta y\Delta z,A_y=\Delta x\Delta z,A_z=\Delta x\Delta y,\Delta V=\Delta x\Delta y\Delta z$$

and

$$b=-[a_E+a_W+a_T+a_B+a_S+a_N-1]H_p^o+b_ES_E+b_WS_W+b_TS_T+b_BS_B+b_SS_S+b_NS_N-b_pS_P+\frac{dt}{\rho}q\Delta V$$

Where:

$$b_E=\frac{\Delta t}{\rho\Delta V}\frac{A_x}{\delta x_e},b_W=\frac{\Delta t}{\rho\Delta V}\frac{A_x}{\delta x_w},b_T=\frac{\Delta t}{\rho\Delta V}\frac{A_y}{\delta y_t},b_B=\frac{\Delta t}{\rho\Delta V}\frac{A_y}{\delta y_b},b_S=\frac{\Delta t}{\rho\Delta V}\frac{A_z}{\delta y_z},b_N=\frac{\Delta t}{\rho\Delta V}\frac{A_z}{\delta y_z}$$

And

$$b_p=b_E+b_W+b_T+b_B+b_S+b_N \quad (21)$$

Where, H_p^o representing the old value of *H* at grid point P

Return to Equation (20), the term b will be considered as zero in case of solid phase (without phase change).

The domain mesh wall is 58×21×20 in x, y, z directions, with time step of 0.5 second. SIMPLE algorithm is used to solve Navier Stokes and energy equations, with hybrid difference scheme.

3 INITIAL AND BOUNDARY CONDITIONS

2.1 Initial Conditions

Initially, the entire domain set to be at ambient temperature, which is equal to (25°C).

2.2 Boundary Conditions

All the velocity components at the wall surface are set to be zero (no slip condition).

Inlet boundary conditions for velocity and temperature: $u=u_{in}$, $T=T_{in}$.

Inlet boundary conditions for turbulence model is$k_{in}=C_k u_{in}^2$, $\varepsilon_{in}=\frac{C_\mu k_{in}^{3/2}}{0.5D_hC_\varepsilon}$

And $C_k=0.003$and $C_\varepsilon=0.03$ [26].

Outlet boundary conditions $\frac{\partial\varphi}{\partial n}=0$, φ:: represents the independent variables, n: normal vector on the outlet section, i.e. x.

3 VALIDITY FOR THE PRESENT CODE

In order to validate the present code, the numerical results were compared with experimental results of Moradi et al. [27] in the same operation condition. Fig.2. represents this comparison. From figure it is noted that there is a good agreement.

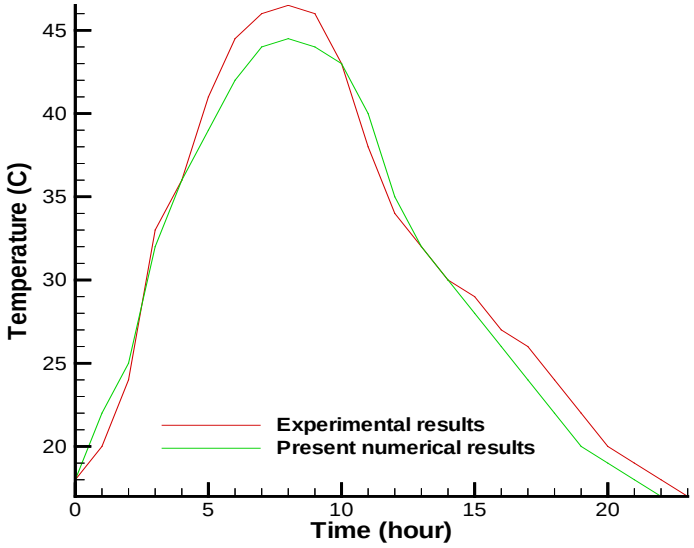

Fig. 2. Comparison between present numerical results with previous experimental results of Moradi et al [27]

4 RESULTS AND DISCUSSION

In order to determine the optimal design of a Trombe wall that utilizes wax as a PCM, several designs have been numerically tested. Where the effect of the thickness of PCM layer was studied and results were found for (2,3,4 and 5) cm over a period of 35 hours to cover all day hours especially at night as well as the middle of the next day. The study was conducted according to weather data for 15th December for Baghdad – Iraq (location: 33.3152° N, 44.3661° E). Results will be discussed in the following paragraphs.

Fig. 3 shows the relationship between the average wax temperatures over 25 hours. It is worth noting that the horizontal axis (time axis) in the following figures expresses the test hours starting from 8 am, which represents (1) for the time axis and thus 25 represents 8 am for the next day. From the figure, one can notice that the temperature of the wax begins to rise as a result of increase in solar radiation to reach its highest value of 37 °C at 12 pm for a 5 cm thick wax while a 2 cm thickness recorded the shortest time to reach the highest temperature, approximately 40 °C after one hour of the beginning of the time (9 am).

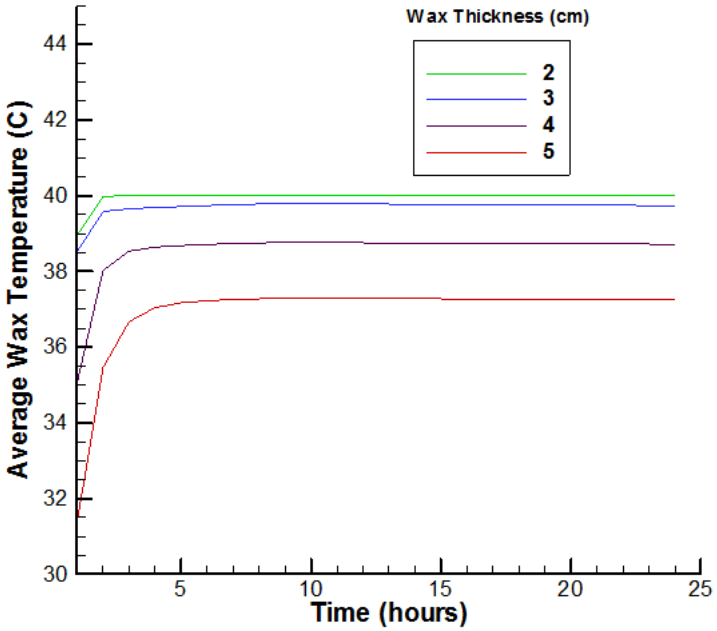

Fig. 3. Average wax temperature within 25 hours for different wax thickness with time interval from 8 am to 8 am next day

Fig. 4 shows the average temperature of the wax during 35 hours. From this figure, there is a stability of the temperature of the wax of a thickness of 2 cm at the highest degree of 40 °C, as it continued at the same temperature during the 35 hours, because wax had absorbed a large amount of sun light heat during the daytime and then released this heat at the nighttime. The absorbed heat converts all the wax from a solid to liquid state during the

phase change process when the temperature reaches the wax melting point, this process will be completed faster for a wax of a minimum thickness of 2 cm compared with other thicknesses. The peak temperature of the wax was 40 °C and remains constant throughout the night, until all the wax has been changed from a liquid to a solid state, while there is a slight decrease in temperature for the other wax thicknesses (3, 4 and 5) cm especially in the early morning hours (4 am), as a result of a large amount of wax for these thicknesses and lower temperature compared with 2 cm thick wax.

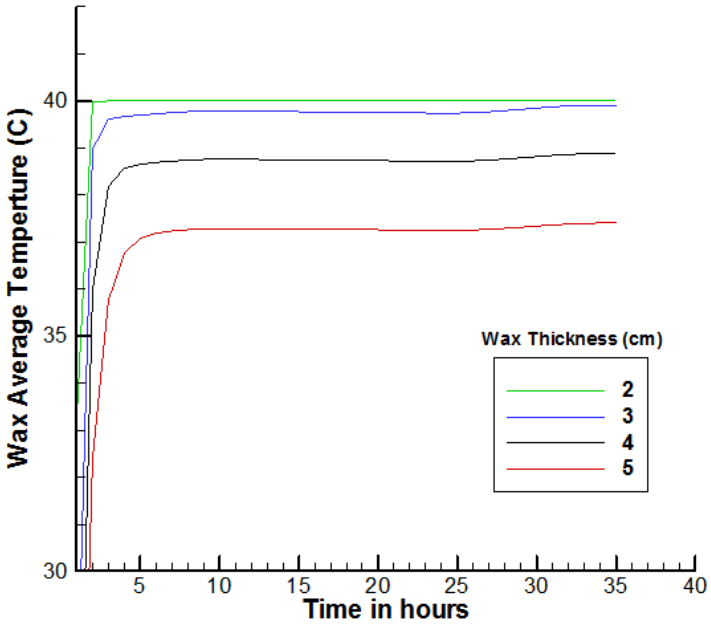

Fig. 4. Average wax temperature within 35 hours for different wax thickness with time interval from 8 am to 11 pm next day

Fig. 5 shows the variation in the average air temperature at exit with the change of time within 35 hours for the four different designs for wax thickness, where it was noted that the highest temperature was recorded at 2 pm and the lowest value was at 8 am for the next day. From the figure, one can notice that the highest and lowest temperature values for 2 cm wax thickness were (29.5 and 22) °C respectively, while for 5 cm wax thickness (28.5 and 21.2) °C respectively, and there is a slight rise in temperatures for the second day of their values for the first day, due to the heat stored in the wax.

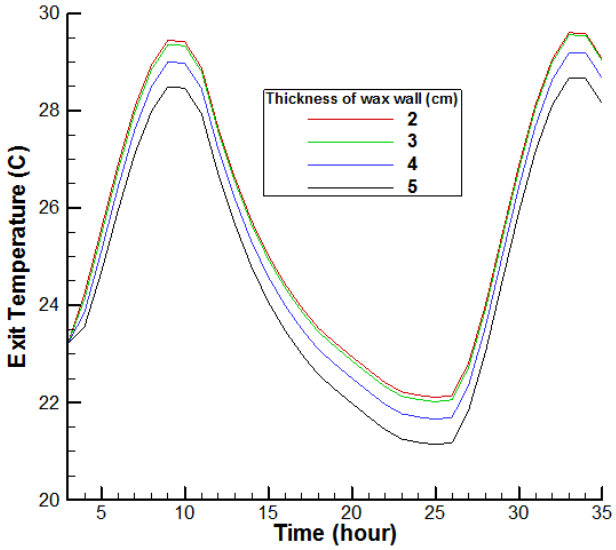

Fig. 5. Exit temperature within 35 hours for different wax thickness with time interval from 8 am to 11 pm next day

Figs. (6-10) represent the temperature contour through the wax material of the four walls (2, 3, 4 and 5) cm thickness at the times of the day (10 am, 12 pm, 5 pm, 10 pm and 7 am for the next day) respectively. From these figures, one can noticed that the highest wax temperature reached was 40 °C for all cases, and it was noticed that there was homogeneity in the temperatures of the wax with thickness (2 and 3) cm, while the temperature varied between the highest and lowest value in the others.

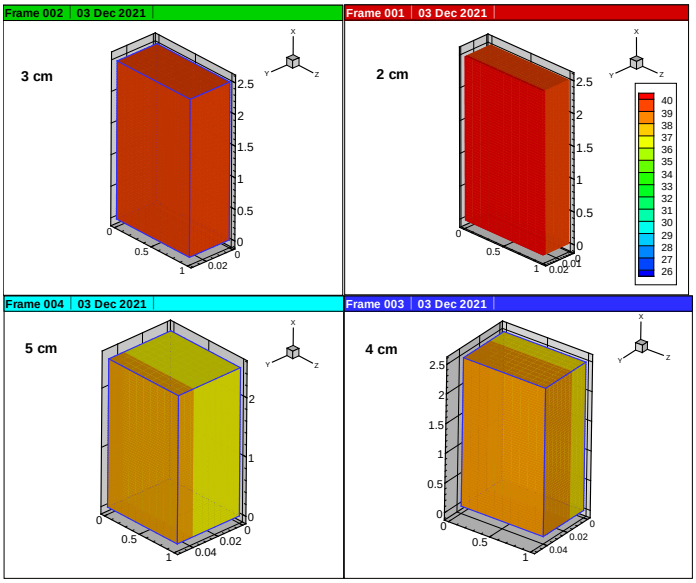

Fig. 6. Wax temperature contour at 10 am

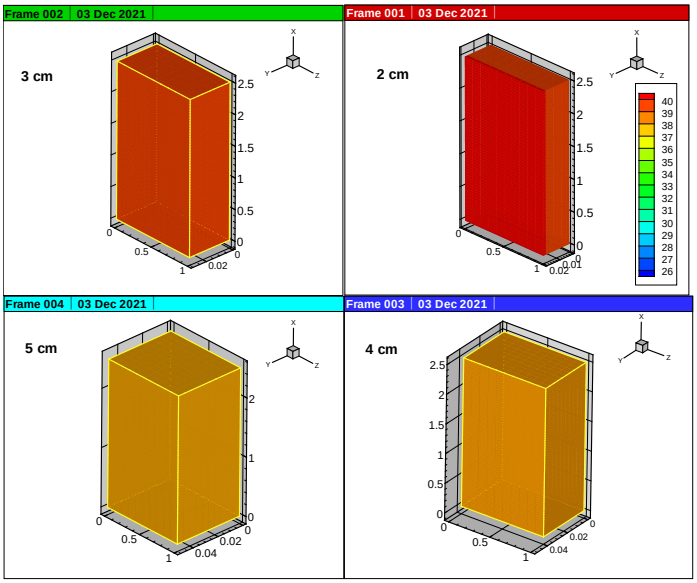

Fig. 7. Wax temperature contour at 12 pm

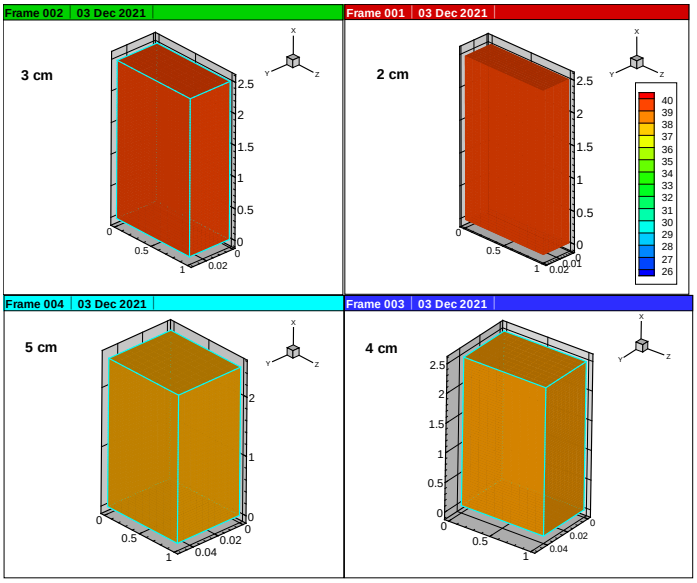

Fig. 8. Wax temperature contour at 5 pm

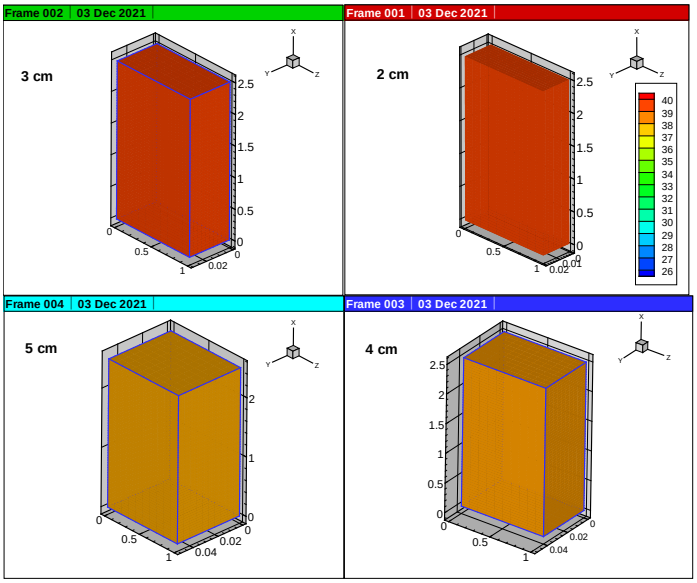

Fig. 9. Wax temperature contour at 10 pm

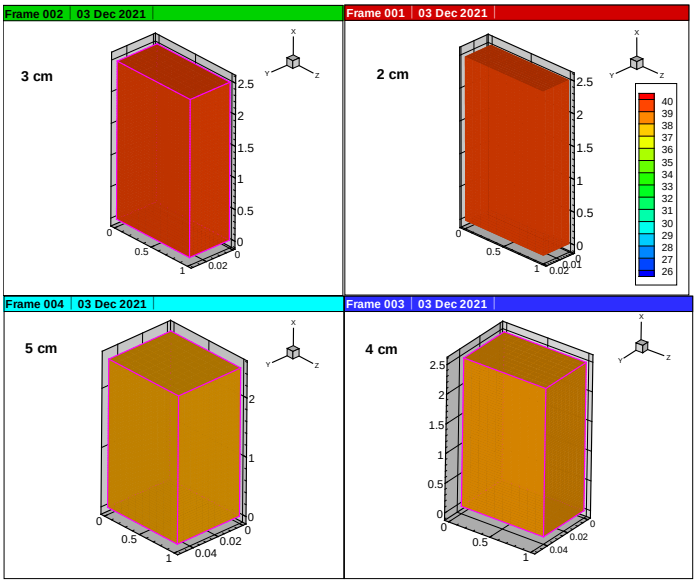

Fig. 10. Wax temperature contour at 7 am, next day

Figs. (11-14) represent the temperature contour for air moving through the air gap between glass and absorber plates for the four walls (2, 3, 4 and 5) cm thickness at the times of the day (10 am, 12 pm, 5 pm, and 7 am for the next day) respectively. From these figures it can be seen that the highest air temperature was in the layer in contact with the absorber plate. As in the previous figures, the thickness (2 and 3) cm was the highest in the temperature values at the exit.

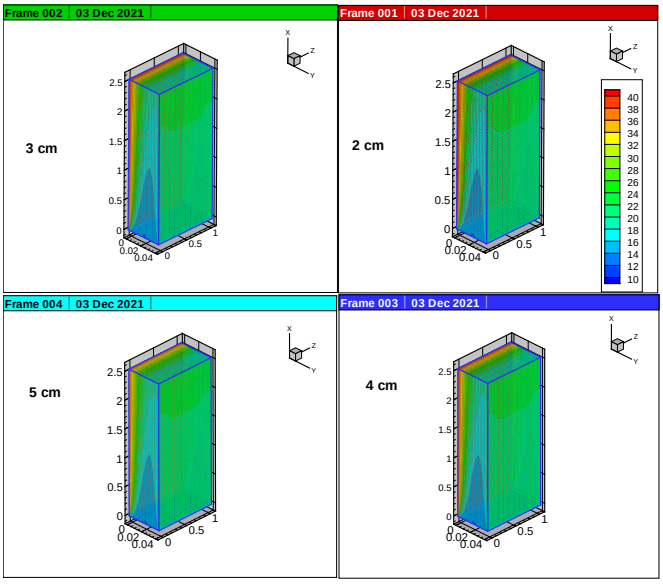

Fig. 11. Temperature contour for air at 10 am

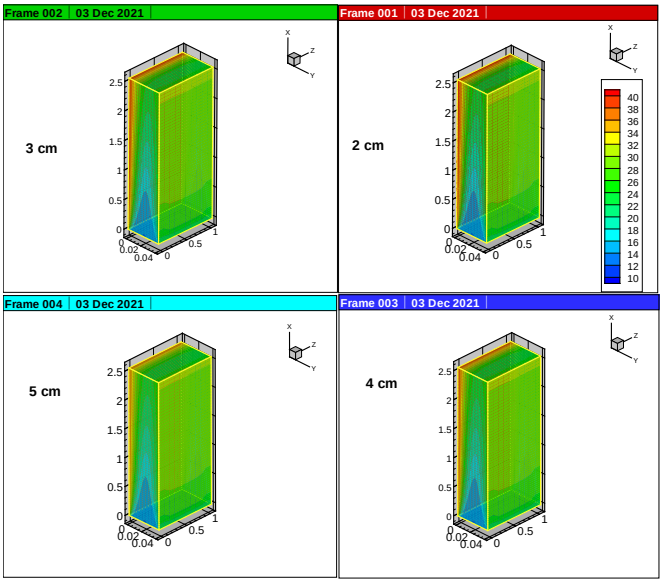

Fig. 12. Temperature contour for air at 12 pm

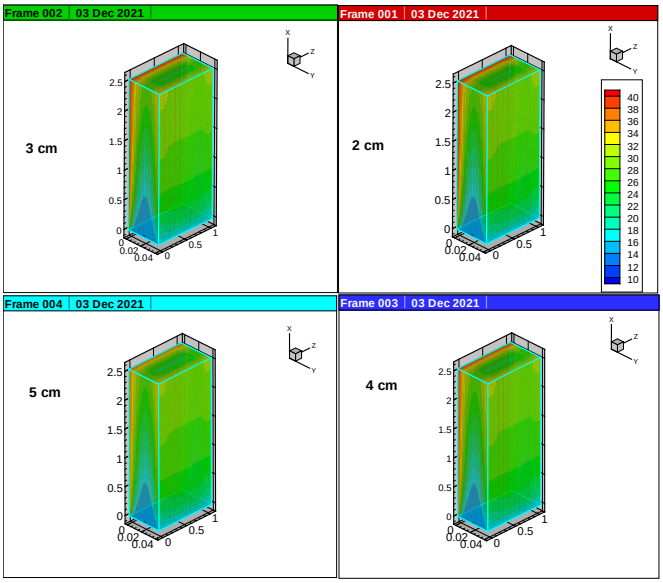

Fig. 13. Temperature contour for air at 5 pm

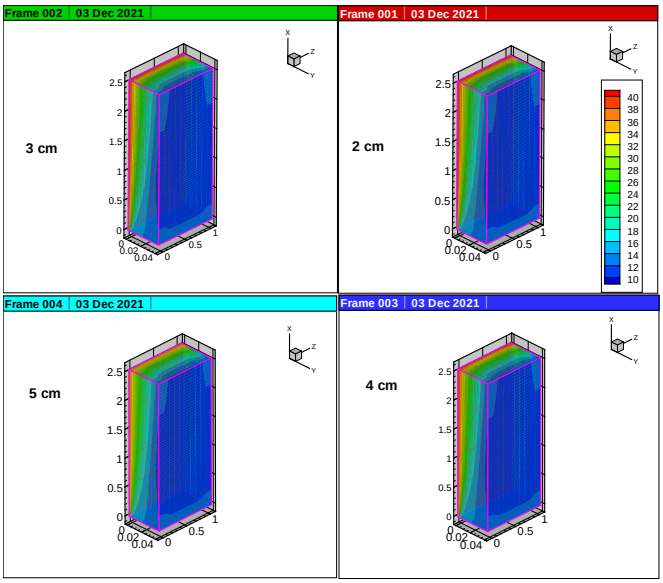

Fig. 14. Temperature contour for air at 7 am, next day

Fig. 15 shows meteorological data for 15th and 16th December in Baghdad, which represents the variation of solar radiation and ambient temperature within 35 hours. By Comparing Figs. 5 and 15, it can be seen that the percentage of the rate of air temperature increases at exit from their values of ambient for wax thickness 2 cm at times (10 am, 12 pm, 5 pm, 10 pm and 7 am for the next day) were (37.8, 19.5, 30.7, 60 and 69.2) % respectively, while they were for wax thickness of 5 cm at the same times (33.5, 15.2, 25.9, 53.3 and 65.3) % respectively.

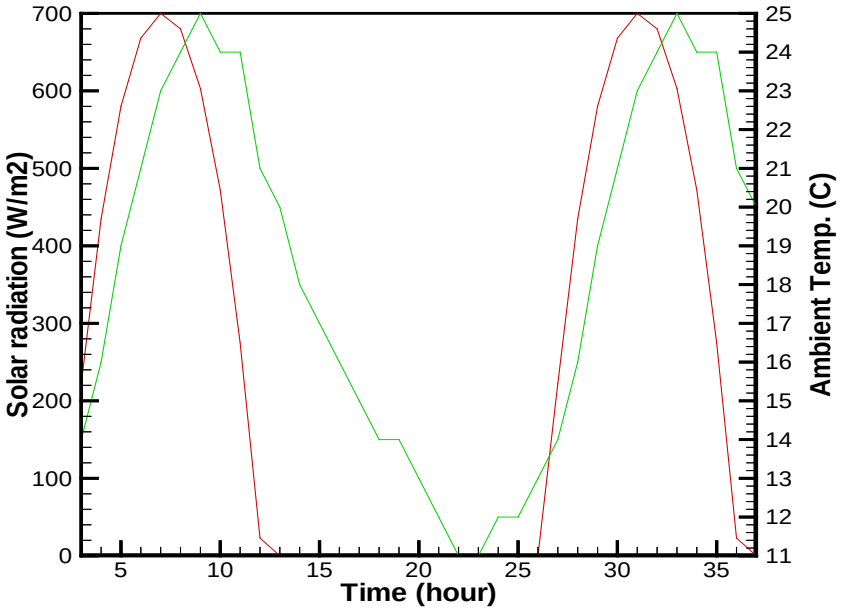

Fig. 15. Meteorological data for 15 and 16 December in Baghdad (Iraqi Meteorological Organization and Seismology) [28]

From all of the above, it is clear that wax thickness of 2 cm is optimal, being the least massive of PCM and the most thermally performance.

5 CONCLUSIONS

Thermal performance of Trombe wall utilizing PCM has been studied numerically. A FORTRAN-90 computer program was built to solve the three-dimensional turbulent Navier stokes and energy equations in additional to enthalpy transforming method for PCM with explicit scheme based on finite volume method. The validity of the present program was checked by comparing the numerical results with the results of a previous experimental study. From the results obtained for different wax thicknesses (2, 3, 4 and 5) cm, it was found that wax thickness of 2 cm is an optimal design. It achieved the highest percentages in the rate of air temperature increase at exit compared with their values of ambient temperature throughout the day, especially at night as (37.8, 19.5, 30.7, 60 and 69.2)% at (10 am, 12 pm, 5 pm, 10 pm and 7 am of the next day) respectively.

6 REFERENCES

[1] Peng, C., Yan, D., Guo, S., Hu, S., & Jiang, Y. (2015). Building energy use in China: ceiling and scenario. *Energy and Buildings*, *102*, 307-316. DOI: 10.1016/j.enbuild.2015.05.049

[2] Abbas, H., Jalil, J. M., & Ahmed, S. T. (2021). Experimental Investigation of The Optimal Location of PCM Capsules in a Hollow Brick Wall. *Engineering and Technology Journal*, *39*(5), 846-858. DOI: 10.30684/etj.v39i5A.1980

[3] Liu, Y., Yang, L., Zheng, W., Liu, T., Zhang, X., & Liu, J. (2018). A novel building energy efficiency evaluation index: Establishment of calculation model and application. *Energy Conversion and Management*, *166*, 522-533. DOI: 10.1016/j.enconman.2018.03.090

[4] Mao, P., Li, J., Tan, Y., Qi, J., & Xiong, L. (2018). Regional suitability of climate-responsive technologies for buildings based on expert knowledge: A China study. *Journal of Cleaner Production*, *204*, 158-168. DOI: 10.1016/j.jclepro.2018.08.274

[5] Liu, J., Liu, Y., Yang, L., Liu, T., Zhang, C., & Dong, H. (2020). Climatic and seasonal suitability of phase change materials coupled with night ventilation for office buildings in Western China. *Renewable Energy*, *147*, 356-373. DOI: 10.1016/j.renene.2019.08.069

[6] Liu, Y., Hou, L., Yang, Y., Feng, Y., Yang, L., & Gao, Q. (2020). Effects of external insulation component on thermal performance of a Trombe wall with phase change materials. *Solar Energy*, *204*, 115-133. DOI: 10.1016/j.solener.2020.04.010

[7] Elghamry, R., & Hassan, H. (2020). Experimental investigation of building heating and ventilation by using Trombe wall coupled with renewable energy system under semi-arid climate conditions. *Solar Energy*, *201*, 63-74. DOI: 10.1016/j.solener.2020.02.087

[8] Wu, S. Y., Xu, L., & Xiao, L. (2020). Performance study of a novel multi-functional Trombe wall with air purification, photovoltaic, heating and ventilation. Energy Conversion and Management, 203, 112229. DOI: 10.1016/j.enconman.2019.112229

[9] Salih, S. M., Jalil, J. M., & Najim, S. E. (2020). Comparative study of novel solar air heater with and without latent energy storage. *Journal of Energy Storage*, *32*, 101751. DOI: 10.1016/j.est.2020.101751

[10] Hu, Z., Zhang, S., Hou, J., He, W., Liu, X., Yu, C., & Zhu, J. (2020). An experimental and numerical analysis of a novel water blind-Trombe wall system. *Energy Conversion and Management*, *205*, 112380. DOI: 10.1016/j.enconman.2019.112380

[11] Wu, S. Y., Yan, X. Q., & Xiao, L. (2020). Numerical analysis on geometric and shape parameters of solar dual-catalytic Trombe wall performance. *Solar Energy*, *199*, 460-473. DOI: 10.1016/j.solener.2020.02.058

[12] Omara, A. A., & Abuelnuor, A. A. (2020). Trombe walls with phase change materials: A review. *Energy Storage*, *2*(6), e123. DOI: 10.1002/est2.123

[13] [13] Lohmann, V., & Santos, P. (2020). Trombe wall thermal behavior and energy efficiency of a light steel frame compartment: Experimental and numerical assessments. *Energies*, *13*(11), 2744. DOI: 10.3390/en13112744

[14] [14] Zhou, L., Huo, J., Zhou, T., & Jin, S. (2020). Investigation on the thermal performance of a composite Trombe wall under steady state condition. *Energy and Buildings*, *214*, 109815. DOI: 10.1016/j.enbuild.2020.109815

[15] [15] Hu, Z., Zhang, S., Hou, J., He, W., Liu, X., Yu, C., & Zhu, J. (2020). An experimental and numerical analysis of a novel water blind-Trombe wall system. *Energy Conversion and Management*, *205*, 112380. DOI: 10.1016/j.enconman.2019.112380

[16] Hong, X., Leung, M. K., & He, W. (2019). Effective use of venetian blind in Trombe wall for solar space conditioning control. *Applied Energy*, *250*, 452-460. DOI: 10.1016/j.apenergy.2019.04.128

[17] Ahmed, O. K., Hamada, K. I., & Salih, A. M. (2019). Enhancement of the performance of Photovoltaic/Trombe wall system using the porous medium: Experimental and theoretical study. *Energy*, *171*, 14-26. DOI: 10.1016/j.energy.2019.01.001

[18] [18] Sá, A. B., Boaventura-Cunha, J., Lanzinha, J. C., & Paiva, A. (2017). An experimental analysis of the Trombe wall temperature fluctuations for high range climate conditions: Influence of ventilation openings and shading devices. *Energy and Buildings*, *138*, 546-558. DOI: 10.1016/j.enbuild.2016.12.085

[19] Midland Refineries Company MRC / Daura Refineries, Ministry of Oil, Iraq.

[20] Jalil, J. M., & Salih, S. M. (2020). Analysis of Thermal and Insulation Performance of Double Glazed Window Doped With Paraffin Wax. *Engineering and Technology Journal*, *38*(3), 383-393. DOI: 10.30684/etj.v38i3A.448

[21] Launder, Brian Edward, and Dudley Brian Spalding. (1983) "The numerical computation of turbulent flows." In Numerical prediction of flow, heat transfer, turbulence and combustion, pp. 96-116. Pergamon,

[22] Abbas, H. M., Jalil, J. M., & Ahmed, S. T. (2021). Experimental and numerical investigation of PCM capsules as insulation materials inserted into a hollow brick wall. *Energy and Buildings*, *246*, 111127. DOI: 10.1016/j.enbuild.2021.111127

[23] Jalil, J. M., & Salih, S. M. (2021). Experimental and numerical investigation of paraffin wax as thermal insulator in a double glazed window. *Journal of Energy Storage*, *35*, 102173. DOI: 10.1016/j.est.2020.102173

[24] Salih, S. M., Jalil, J. M., & Najim, S. E. (2019). Experimental and numerical analysis of double-pass solar air heater utilizing multiple capsules PCM. *Renewable Energy*, *143*, 1053-1066. DOI: 10.1016/j.renene.2019.05.050

[25] Suffer, K. H., Jalil, J. M., & Hasan, H. A. (2020). Numerical investigation of PCM thermal storage in water solar collector. *Journal of Advanced Research in Fluid Mechanics and Thermal Sciences*, *66*(1), 164-178.

[26] J M. Jalil, A. H. Ayaal, S. S. Faris (2011). Economic Energy Consumption Using Tromb Wall Without Openings By Solar Radiation. Engineering and Technology Journal, 29(8).

[27] Moradi, R., Kianifar, A., & Wongwises, S. (2017). Optimization of a solar air heater with phase change materials: Experimental and numerical study. *Experimental Thermal and Fluid Science*, *89*, 41-49. DOI: 10.1016/j.expthermflusci.2017.07.011

[28] Iraqi Meteorological Organization and Seismology, http://meteoseism.gov.iq/

Paper submitted: 16.03.2022.
Paper accepted: 25.05.2022.